

# Notes on the Ward BRDF

Bruce Walter\*

Technical Report PCG-05-06  
 Cornell Program of Computer Graphics  
 April 29, 2005

## Abstract

The anisotropic BRDF introduced in [Ward 1992] has become widely used in computer graphics, but some important implementation details are less widely known. We discuss how to efficiently evaluate the Ward BRDF. Then we derive the probability density function for its associated Monte Carlo sampling scheme and the correct weights to use with the generated samples. Finally for the isotropic version, we describe how to bound the maximum possible BRDF value over a region of (direction) space.

## 1 Introduction

The Ward BRDF (Bidirectional Reflectance Distribution Function) was introduced in [Ward 1992] as an empirical model to fit measured BRDF (i.e. surface reflectance) data. It has several advantages over the prior BRDF models and has become widely used in the computer graphics community. It uses only a few simple parameters making it easy to control, can be sampled efficiently for Monte Carlo, can model anisotropic surfaces, and was shown to fit reasonably well to measured BRDF data.

The purpose of this paper is to clarify and correct some important implementation details of the Ward BRDF. We discuss how to efficiently evaluate the BRDF in Section 2. Monte Carlo BRDF sampling is required for many rendering algorithms, and hence, Ward provided an efficient sampling scheme with his BRDF. However he did not provide the associated probability density function, which for mathematical accuracy, is needed to correctly weight the generated samples. We both discuss how to derive such probability density functions in general in Section 3, and present the specific results for the Ward BRDF in Equation 10.

Another powerful, though less widely used, BRDF operation is the ability to bound its maximum value over a range of directions. In Section 4, we discuss how to cheaply and tightly bound the isotropic Ward BRDF over a set of directions defined by a spatial bounding volume.

### 1.1 Notation

We will be working extensively with directions in 3D, which we will denote in boldface (e.g.,  $\mathbf{v}$ ). In actual use, these directions are typically represented as normalized 3D vectors (e.g.,  $\mathbf{v} = [v_x, v_y, v_z]$ , where  $v_x^2 + v_y^2 + v_z^2 = 1$ ). Directions can also be represented as two angles,  $\theta$  and  $\phi$ , using spherical polar coordinates as illustrated in Figure 1. We will usually subscript these angles with the direction that they are describing. We can convert between the spherical angles and the 3D unit vector representations using:

$$(\theta, \phi) \Leftrightarrow [\sin \theta \cos \phi, \sin \theta \sin \phi, \cos \theta] \quad (1)$$

The scalar dot product of two directions is equal to the cosine of the angle between them (e.g.,  $\mathbf{v} \cdot \mathbf{z} = \cos \theta_v$ ). When using 3D vectors, the dot product can be computed by summing the products of the corresponding components (e.g.,  $\mathbf{u} \cdot \mathbf{v} = u_x v_x + u_y v_y + u_z v_z$ ).

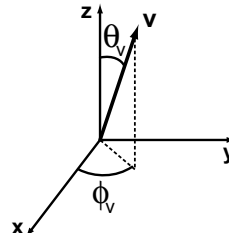


Figure 1: Spherical polar coordinates example. The direction  $\mathbf{v}$  can be fully described by two angles  $\theta_v$  and  $\phi_v$ .  $\theta_v$  is the angle between  $\mathbf{v}$  and the z-axis.  $\phi_v$  is the angle between the x-axis and  $\mathbf{v}$ 's projection onto the x-y plane.

A BRDF (Bidirectional Reflectance Distribution Function) describes how light is scattered at a surface. At a surface point it is a function of two directions (an incident direction  $\mathbf{i}$  and an outgoing direction  $\mathbf{o}$ ) and written as  $f_r(\mathbf{i}, \mathbf{o})$ . It is often convenient to construct a coordinate frame on the surface where the z-axis is the same of the local surface normal,  $\mathbf{n}$ , and the x and y axes lie in the tangent plane of the surface as shown in Figure 2. For anisotropic BRDFs, the x and y axes must match the principle directions of anisotropy, while they can be chosen arbitrarily for isotropic BRDFs.

The Ward BRDF uses the half direction  $\mathbf{h}$  that is defined to be halfway between the incident and out directions. It can be computed by adding  $\mathbf{i}$  and  $\mathbf{o}$  as 3D vectors and then renormalizing:

$$\mathbf{h} = \frac{\mathbf{i} + \mathbf{o}}{\|\mathbf{i} + \mathbf{o}\|} \quad (2)$$

The half angle is motivated by microfacet BRDFs and produces more realistic highlights than alternatives such as Phong (e.g., see [Fisher 1994; Ngan et al. 2004]).

## 2 Ward BRDF

The original Ward BRDF is defined as the sum of two components [Ward 1992, Equation 5a]. The first is a diffuse term,  $\rho_d/\pi$ . Diffuse components are relatively simple and already well understood, so we will ignore the diffuse component for the remainder of this paper. The second component is a gaussian anisotropic gloss lobe defined by three parameters,  $\rho_s$ ,  $\alpha_x$ , and  $\alpha_y$ , as:

$$f_r(\mathbf{i}, \mathbf{o}) = \frac{\rho_s}{4\pi\alpha_x\alpha_y\sqrt{\cos\theta_i\cos\theta_o}} e^{-\tan^2\theta_h\left(\frac{\cos^2\phi_h}{\alpha_x^2} + \frac{\sin^2\phi_h}{\alpha_y^2}\right)} \quad (3)$$

where  $\rho_s$  controls the magnitude of the lobe, and  $\alpha_x$  and  $\alpha_y$  control the width of the lobe in the two principal directions of anisotropy. If  $\alpha_x = \alpha_y$  then the lobe is isotropic (i.e. invariant under surface rotations around the surface normal).

Just after defining his BRDF, Ward presents an approximation that is intended to be computationally cheaper [Ward 1992, Equation 5b]. There is no reason to ever use this approximation. The following vector equation is both exact and cheaper to compute than

\*email: bjw@graphics.cornell.edu

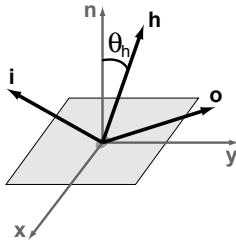


Figure 2: Coordinate frame used in BRDF calculations. The z-axis is equal to the local surface normal  $\mathbf{n}$ , and the x and y axes lie in the surface's tangent plane. The BRDF is a function of two directions, the incident direction,  $\mathbf{i}$ , and out direction  $\mathbf{o}$  (e.g., the directions to the eye and light). The half direction  $\mathbf{h}$  is defined to lie midway between  $\mathbf{i}$  and  $\mathbf{o}$ , and plays an important role in the Ward BRDF.

the approximation<sup>1</sup>.

$$f_r(\mathbf{i}, \mathbf{o}) = \frac{\rho_s}{4\pi\alpha_x\alpha_y\sqrt{(\mathbf{i}\cdot\mathbf{n})(\mathbf{o}\cdot\mathbf{n})}} e^{-\frac{((\mathbf{h}\cdot\mathbf{x})/\alpha_x)^2 + ((\mathbf{h}\cdot\mathbf{y})/\alpha_y)^2}{(\mathbf{h}\cdot\mathbf{n})^2}} \quad (4)$$

Since  $\mathbf{h}$  appears to equal powers in both the numerator and denominator of the exponent, an unnormalized half vector can be used when evaluating this equation. It is trivial to show that Equations 3 and 4 are equivalent by expressing  $\mathbf{h}$  as a 3D unit vector as shown below and expanding the dot products.

$$\mathbf{h} = [\sin\theta_h \cos\phi_h, \sin\theta_h \sin\phi_h, \cos\theta_h] \quad (5)$$

## 2.1 Sampling

A good BRDF sampling technique is essential in the efficiency of Monte Carlo rendering algorithms. When sampling, we regard the incident vector  $\mathbf{i}$  as given, or fixed, and want to generate out vectors  $\mathbf{o}$  in a distribution that closely matches the BRDF. Ward provided a sampling for his BRDF [Ward 1992, Equation 7], but accidentally omitted an arctangent in his equations<sup>2</sup>. Given two uniform random variables  $u$  and  $v$  in the range  $0 < u, v < 1$ , the correct sampling equations are:

$$\theta_h = \arctan \sqrt{\frac{-\log u}{\cos^2\phi_h/\alpha_x^2 + \sin^2\phi_h/\alpha_y^2}} \quad (6)$$

$$\phi_h = \arctan\left(\frac{\alpha_y}{\alpha_x} \tan(2\pi v)\right) \quad (7)$$

Care must be taken in computing the second arctangent to keep  $\phi_h$  in the same quadrant as the angle  $2\pi v$ . These sampling equations compute the half direction  $\mathbf{h}$  from  $u$  and  $v$ , which is then used to generate direction  $\mathbf{o}$  from  $\mathbf{h}$  and  $\mathbf{i}$  using:

$$\mathbf{o} = 2(\mathbf{i}\cdot\mathbf{h})\mathbf{h} - \mathbf{i} \quad (8)$$

If the generated distribution of out directions  $\mathbf{o}$  perfectly matches the BRDF, then all the samples can be given the same weight. However, this is rarely the case for non-trivial BRDFs. In order to compute the correct sampling weights we need to know the actual prob-

<sup>1</sup>This vector form has been independently found by multiple people including myself. Greg Ward credits Christophe Schlick as being the first. Equivalent formulations can also be found in [Ward 2004] and recent versions of [Larson and Shakespeare 2004].

<sup>2</sup>Missing arctangent was first reported to Greg Ward by Alex Keller and can also be found in [Dutre 2001]

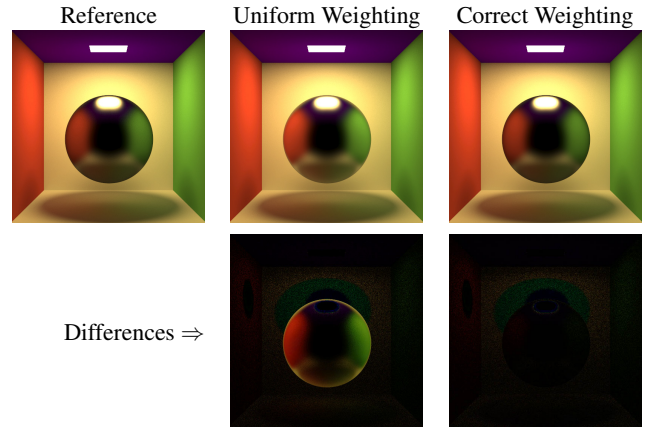


Figure 3: Shown here is a diffuse box containing a sphere with a Ward BRDF ( $\rho_s = 0.75, \alpha_x = \alpha_y = 0.15$ ). The left image is a reference solution that used uniform hemisphere sampling. The middle image used Ward's sampling but assumed uniform weights ( $w(\mathbf{o}) = \rho_s$ ), while the right image used the correct sample weights (Equation 10). The bottom row shows the differences between the images with Ward's sampling and the reference.

ability density function  $p_o$  for the generated directions  $\mathbf{o}$ . The correct probability function from the Ward sampling is:

$$p_o(\mathbf{o}) = \frac{1}{4\pi\alpha_x\alpha_y(\mathbf{h}\cdot\mathbf{i})\cos^3\theta_h} e^{-\tan^2\theta_h\left(\frac{\cos^2\phi_h}{\alpha_x^2} + \frac{\sin^2\phi_h}{\alpha_y^2}\right)} \quad (9)$$

This probability is, by design, quite close to the Ward BRDF (see Equation 3), but does not exactly match it. The next section will describe how to find sampling probability functions and how to derive Equation 9. The correct weighting function  $w(\mathbf{o})$  that should be applied to the samples in Monte Carlo algorithms (e.g., path tracing) is given by:

$$w(\mathbf{o}) = \frac{f_r(\mathbf{i}, \mathbf{o}) \cos\theta_o}{p_o(\mathbf{o})} = \rho_s (\mathbf{h}\cdot\mathbf{i}) (\mathbf{h}\cdot\mathbf{n})^3 \sqrt{\frac{(\mathbf{o}\cdot\mathbf{n})}{(\mathbf{i}\cdot\mathbf{n})}} \quad (10)$$

Previous work has generally assumed that the samples of the Ward BRDF could be equally weighted (i.e.  $w(\mathbf{o}) \approx \rho_s$ ). This is often nearly true, but can cause significant errors for wide lobes and for angles near grazing as demonstrated in Figure 3. To get the correct results in these cases, one needs to use the correct sampling weights from Equation 10.

Some viewers may aesthetically prefer the middle image in Figure 3, but it is the left and right images that are mathematically correct for the Ward BRDF. The darkening effect near grazing is built into the Ward BRDF definition. [Duer 2005] has proposed modifying its equations to reduce this effect, however that lies beyond the scope of this paper.

## 3 Deriving Sampling Probabilities

In this section we will review how to derive the probability density for a given sampling transform and demonstrate how to use this theory to find the probability function for the isotropic case of the Ward BRDF. We are specifically interested in 2D probability densities here, but similar relations hold for other dimensions.

### 3.1 General Theory

Let  $S$  be our 2D source space and  $[s_1, s_2] \in S$  be a random variable with known probability density  $p_s$ . Given a target space  $T$ , any transform from  $S$  to  $T$  defines a new random variable  $[t_1, t_2] \in T$  (where  $t_1 = t_1(s_1, s_2)$  and  $t_2 = t_2(s_1, s_2)$ ). We want to compute the probability density  $p_t$  associated with the transformed random variable,  $[t_1, t_2]$ .

For simplicity we will assume the transform is invertible over the regions of interest (i.e. we can also write  $s_1 = s_1(t_1, t_2)$  and  $s_2 = s_2(t_1, t_2)$ ). The probability of the random variable being in a region  $B$  (which we write as  $P(B)$ ) is given by integrating its probability density over that region with respect to its associated measure (e.g.,  $p_t$  and its measure  $dt_1 dt_2$ ).

$$P(B) = \int_B p_t(t_1, t_2) dt_1 dt_2 \quad (11)$$

A probability density must always have an associated measure, though often the associated measure is implicit. Given a region  $B \subseteq T$ , let  $A_B \subseteq S$  be the set of all points in  $S$  that map to points in  $B$ . The probabilities of these two sets must be equal (i.e.  $P(A_B) = P(B)$ ) since they cover the same events, and thus we have:

$$\int_{A_B} p_s(s_1, s_2) ds_1 ds_2 = \int_B p_t(t_1, t_2) dt_1 dt_2 \quad (12)$$

By applying the change of variables theorem from calculus to the first integral, we get:

$$\int_{A_B} p_s(s_1, s_2) ds_1 ds_2 = \int_B p_s(s_1(t_1, t_2), s_2(t_1, t_2)) \left\| \frac{\partial [s_1, s_2]}{\partial [t_1, t_2]} \right\| dt_1 dt_2 \quad (13)$$

where the absolute value of the determinant of the Jacobian is defined in terms of partial derivatives as:

$$\left\| \frac{\partial [s_1, s_2]}{\partial [t_1, t_2]} \right\| = \left\| \begin{array}{cc} \frac{\partial s_1}{\partial t_1} & \frac{\partial s_1}{\partial t_2} \\ \frac{\partial s_2}{\partial t_1} & \frac{\partial s_2}{\partial t_2} \end{array} \right\| = \left| \frac{\partial s_1}{\partial t_1} \frac{\partial s_2}{\partial t_2} - \frac{\partial s_2}{\partial t_1} \frac{\partial s_1}{\partial t_2} \right| \quad (14)$$

Since these equations hold for any set  $B$ , we can use them to solve for the probability density  $p_t$  as:

$$p_t(t_1, t_2) = p_s(s_1(t_1, t_2), s_2(t_1, t_2)) \left\| \frac{\partial [s_1, s_2]}{\partial [t_1, t_2]} \right\| \quad (15)$$

### 3.2 Application to $p_h$ and $p_o$

We want to specialize this general theory to handle the specific case of finding probability density functions for sampling methods based on the half direction  $\mathbf{h}$  (such as the Ward BRDF). Such sampling methods take two uniform random numbers  $u$  and  $v$ , transform them into a half direction  $\mathbf{h}$  and then uses  $\mathbf{h}$  to generate the out vector  $\mathbf{o}$ . We will first discuss deriving the probability density  $p_h$  for  $\mathbf{h}$  and then relate this to the probability density  $p_o$  for the out vector  $\mathbf{o}$ .

To start we want to apply Equation 15 where we substitute  $u, v$  for  $s_1, s_2$  and  $\theta_h, \phi_h$  for  $t_1, t_2$ , but there is a small difficulty. We are transforming to a non-Euclidean space, the sphere of directions, and the appropriate measure to use with  $p_h$  is solid angle (i.e. the solid angle measure is  $\sin \theta_h d\theta_h d\phi_h$  rather than just  $d\theta_h d\phi_h$ ). We adjust for this by including an additional factor of  $1/\sin \theta_h$  to cancel out the extra factor in the solid angle measure to get:

$$\begin{aligned} p_h(\mathbf{h}) &= p_{uv}(u(\theta_h, \phi_h), v(\theta_h, \phi_h)) \left\| \frac{\partial [u, v]}{\partial [\theta_h, \phi_h]} \right\| \frac{1}{\sin \theta_h} \\ &= \left| \frac{\partial u}{\partial \theta_h} \frac{\partial v}{\partial \phi_h} - \frac{\partial v}{\partial \theta_h} \frac{\partial u}{\partial \phi_h} \right| \frac{1}{\sin \theta_h} \end{aligned} \quad (16)$$

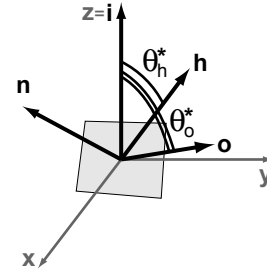


Figure 4: A coordinate system where the incident vector  $\mathbf{i}$  is the  $z$ -axis, and the surface normal  $\mathbf{n}$  lies in the  $x$ - $z$  plane (i.e.  $\mathbf{n} \cdot \mathbf{y} = 0$ ). As in Figure 1, we can specify directions using two spherical angles,  $\theta^*$  and  $\phi^*$ . The star indicates that they are relative to this coordinate frame. The relationship between  $\mathbf{h}$  and  $\mathbf{o}$  is,  $\theta_o^* = 2\theta_h^*$  and  $\phi_o^* = \phi_h^*$ .

where we have used the fact that  $p_{uv}(u, v) = 1$  since  $u$  and  $v$  are uniformly distributed in the unit square.

We will also need to compute  $p_o$  in terms of  $p_h$ . The relationship between  $\mathbf{h}$  and  $\mathbf{o}$  can be expressed very simply by using the special coordinate frame shown in Figure 4, where the incident direction  $\mathbf{i}$  is used as the  $z$ -axis. To clearly distinguish them, we will mark all spherical angles using these special coordinates with a star superscript. The relationship between  $\mathbf{h}$  and  $\mathbf{o}$  in these coordinates is simple:  $\theta_o^* = 2\theta_h^*$  and  $\phi_o^* = \phi_h^*$ . We can once again apply Equation 15, with slight modification again for using solid angle measures, to get:

$$\begin{aligned} p_o(\mathbf{o}) &= p_h(\mathbf{h}) \left\| \frac{\partial [\theta_h^*, \phi_h^*]}{\partial [\theta_o^*, \phi_o^*]} \right\| \frac{\sin \theta_h^*}{\sin \theta_o^*} \\ &= p_h(\mathbf{h}) \left| \frac{1}{2} - 0 \right| \frac{\sin \theta_h^*}{\sin 2\theta_h^*} \\ &= \frac{p_h(\mathbf{h})}{4 \cos \theta_h^*} = \frac{p_h(\mathbf{h})}{4(\mathbf{h} \cdot \mathbf{i})} \end{aligned} \quad (17)$$

Similar results for the half direction to out direction transform can be found in [Torrance and Sparrow 1967] and [Ashikhmin and Shirley 2000].

### 3.3 Isotropic Example

Now to demonstrate how to apply these equations for a specific case, we will derive the sampling probability density for the simpler isotropic case. The Ward BRDF is isotropic when  $\alpha_x = \alpha_y$ , which we can then simply write as  $\alpha$ . In this case the BRDF simplifies to:

$$f_r^{\text{iso}}(\mathbf{i}, \mathbf{o}) = \frac{\rho_s}{4\pi\alpha^2\sqrt{\cos \theta_i \cos \theta_o}} e^{-\frac{\tan^2 \theta_h}{\alpha^2}} \quad (18)$$

and the isotropic sampling equations simplify to:

$$\theta_h = \arctan(\alpha\sqrt{-\log u}) \quad (19)$$

$$\phi_h = 2\pi v \quad (20)$$

We can invert these isotropic sampling equations to get:

$$u = e^{-\frac{\tan^2 \theta_h}{\alpha^2}} \quad (21)$$

$$v = \frac{\phi_h}{2\pi} \quad (22)$$

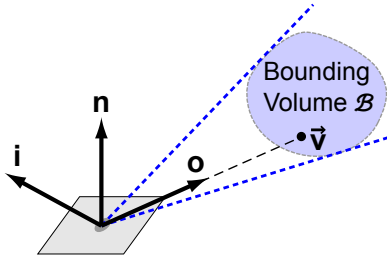


Figure 5: Bounding the maximum BRDF value. The incident and normal directions are fixed and the reflection point is assumed to be at the origin. We then compute an upper bound on  $f_r(\mathbf{i}, \mathbf{o})$  over a set of out directions defined by a bounding volume  $\mathcal{B}$ . The allowed out directions are  $\mathbf{o} = \vec{\mathbf{v}}/\|\vec{\mathbf{v}}\|$  for any  $\vec{\mathbf{v}} \in \mathcal{B}$ .

Then we can apply Equation 16 and compute the partial derivatives of  $u$  and  $v$  with respect to  $\theta_h$  and  $\phi_h$  to get:

$$\begin{aligned} p_h^{\text{iso}}(\mathbf{h}) &= \left| \left( e^{-\frac{\tan^2 \theta_h}{\alpha^2}} \frac{2 \tan \theta_h}{\alpha^2 \cos^2 \theta_h} \right) \left( \frac{1}{2\pi} \right) - (0)(0) \right| \frac{1}{\sin \theta_h} \\ &= \frac{1}{\pi \alpha^2 \cos^3 \theta_h} e^{-\frac{\tan^2 \theta_h}{\alpha^2}} \end{aligned} \quad (23)$$

where we removed the absolute value operation because it is always positive within the valid range of  $\theta_h$ , between zero and  $\pi/2$ . Finally we use Equation 17, we get the probability density for the sampled out direction  $\mathbf{o}$  in the isotropic case as:

$$p_o^{\text{iso}}(\mathbf{o}) = \frac{1}{4\pi \alpha^2 (\mathbf{h} \cdot \mathbf{i}) \cos^3 \theta_h} e^{-\frac{\tan^2 \theta_h}{\alpha^2}} \quad (24)$$

The derivation of Equation 9 for the anisotropic case is performed similarly with verification left as an exercise for the reader.

## 4 Bounding the BRDF

Another useful BRDF operation is bounding its maximum value over a set of directions. While this is a much less common operation than sampling, it is a powerful operation that is required by some rendering algorithms [Walter et al. 2005]. In this section we will describe how to compute a reasonably cheap and tight bound on the isotropic Ward BRDF. Extension to the more general anisotropic version are left as future work.

When bounding the BRDF, the incident direction  $\mathbf{i}$  and the surface point are considered fixed, but the out direction  $\mathbf{o}$  is allowed to vary. We can specify the set of allowed out directions using a bounding volume  $\mathcal{B}$  as shown in Figure 5. For simplicity, let's assume the surface reflection point is at the origin. Let  $\vec{\mathbf{v}}$  be a 3D vector; the arrow indicates it is a vector of arbitrary length rather than a normalized direction. We want to compute an upper bound on a function of  $\mathbf{o}$ , (i.e. the BRDF in our case), over all  $\mathbf{o} = \vec{\mathbf{v}}/\|\vec{\mathbf{v}}\|$  where  $\vec{\mathbf{v}} \in \mathcal{B}$ .

One standard solution would be to use interval arithmetic. By replacing each operator by its interval equivalent and expressing the bounding volume as intervals, computing an upper bound would be straightforward. Unfortunately these interval bounds tend to be rather loose, especially if the initial intervals are large. Instead we will proceed by trying to find a direction or set of parameters that is a strict upper bound and corresponds to a point in or near the bounding volume.

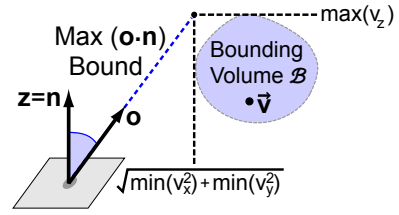


Figure 6: An example of bounding the maximum value of  $\cos \theta_o$  using Equation 27.

### 4.1 Cosine Bound

Let us begin with the relatively simple problem of computing an upper bound on  $\cos \theta_o$  over the bounding volume  $\mathcal{B}$ . If we use a coordinate system where the surface normal  $\mathbf{n}$  is the z-axis (e.g., Figure 2) and let  $\mathbf{o} = \vec{\mathbf{v}}/\|\vec{\mathbf{v}}\|$ , then we can write this as:

$$\cos \theta_o = (\mathbf{o} \cdot \mathbf{z}) = \frac{v_z}{\sqrt{v_x^2 + v_y^2 + v_z^2}} \quad (25)$$

The derivative of  $\cos \theta_o$  with respect to  $v_z$  is always positive, thus we can replace  $v_z$  with its maximum value over the bounding volume  $\mathcal{B}$  to get:

$$\cos \theta_o \leq \frac{\max(v_z)}{\sqrt{v_x^2 + v_y^2 + [\max(v_z)]^2}} \quad (26)$$

Now that the sign of the numerator is fixed, we can select  $v_x$  and  $v_y$  to minimize or maximize the denominator appropriately:

$$\cos \theta_o \leq \begin{cases} \frac{\max(v_z)}{\sqrt{\min(v_x^2) + \min(v_y^2) + [\max(v_z)]^2}} & \text{if } \max(v_z) \geq 0 \\ \frac{\max(v_z)}{\sqrt{\max(v_x^2) + \max(v_y^2) + [\max(v_z)]^2}} & \text{otherwise} \end{cases} \quad (27)$$

An example is shown in Figure 6. Note that we choose the maximum value of  $v_z$  but for  $v_x$  and  $v_y$  we choose the values that maximize or minimize their squared values. Thus if  $v_x$  can vary from -2 to 1, then  $\max(v_x) = 1$ , but  $\max(v_x^2) = 4$  and  $\min(v_x^2) = 0$ .

### 4.2 Isotropic Bound

To bound the isotropic Ward BRDF (Equation 18), we start by bounding its exponential term by computing a lower bound for  $\tan \theta_h$ . Or equivalently, since  $0 \leq \theta_h \leq \pi/2$ , we can compute an upper bound on  $\cos \theta_h = (\mathbf{h} \cdot \mathbf{n})$ . We will use the coordinate system from Figure 4 because of its simple relationship between  $\mathbf{o}$  and  $\mathbf{h}$ . By expressing  $\mathbf{h}$  and  $\mathbf{n}$  as 3D unit vectors based on their spherical coordinates and noting that  $\phi_h^* = 0$ , we get:

$$\begin{aligned} (\mathbf{h} \cdot \mathbf{n}) &= [\sin \theta_h^* \cos \phi_h^*, \sin \theta_h^* \sin \phi_h^*, \cos \theta_h^*] \cdot [\sin \theta_n^*, 0, \cos \theta_n^*] \\ &= \sin \theta_n^* \sin \theta_h^* \cos \phi_h^* + \cos \theta_n^* \cos \theta_h^* \end{aligned} \quad (28)$$

Since  $\theta_n^*$  is fixed, we need only select appropriate values for  $\theta_h^*$  and  $\phi_h^*$  that maximize this expression.

The derivative of  $(\mathbf{h} \cdot \mathbf{n})$  with respect to  $\cos \phi_h^*$  is always positive, so we can replace  $\cos \phi_h^*$  with its maximum value over the bounding volume  $\mathcal{B}$ . Using the coordinate frame of Figure 4 to express the points  $\vec{\mathbf{v}}^* \in \mathcal{B}$  and since  $\phi_h^* = \phi_o^*$  we have:

$$\cos \phi_h^* = \cos \phi_o^* = \frac{v_y^*}{\sqrt{(v_x^*)^2 + (v_y^*)^2}} \quad (29)$$

and we can compute a bound on the maximum of  $\cos \phi_h^*$  in a similar way as we did for Equation 27.

The situation for  $\theta_h^*$  is more complicated. We can compute a bounding interval of possible values for  $\cos \theta_o^*$  using Equation 27 to bound its maximum value and an analogous equation to bound its minimum. Then we can use the half angle formula from trigonometry:

$$\cos \theta_h^* = \cos \frac{\theta_o^*}{2} = \sqrt{\frac{1 + \cos \theta_o^*}{2}} \quad (30)$$

to transform this into an interval bound on  $\cos \theta_h^*$ . To select the appropriate value from this interval, we need to know the value that would maximize  $(\mathbf{h} \cdot \mathbf{n})$ . We can solve for the maximizing value of  $\cos \theta_h^*$  by taking the equation for  $(\mathbf{h} \cdot \mathbf{n})$ , replacing  $\cos \phi_h^*$  by its upper bound, then taking the derivative with respect to  $\theta_h^*$  and setting it equal to zero. The maximizing value of  $\cos \theta_h^*$  is thus given by:

$$\begin{aligned} \frac{\partial(\mathbf{h} \cdot \mathbf{n})}{\partial \theta_h^*} &= 0 \\ \sin \theta_h^* \cos \theta_h^* \max(\cos \phi_h^*) - \cos \theta_h^* \sin \theta_h^* &= 0 \\ \tan \theta_h^* &= \frac{\sin \theta_o^* \max(\cos \phi_h^*)}{\cos \theta_h^*} \\ \cos \theta_h^* &= \begin{cases} \sqrt{\frac{\cos^2 \theta_o^*}{\cos^2 \theta_o^* + \sin^2 \theta_o^* [\max(\cos \phi_h^*)]^2}} & \text{if } \max(\cos \phi_h^*) \geq 0 \\ 1 & \text{otherwise} \end{cases} \end{aligned} \quad (31)$$

where the two cases are needed because when  $\max(\cos \phi_h^*)$  is negative then so is the maximizing angle, but negative values for  $\theta_h^*$  are not allowed and must be clamped to zero. We have also used the identity  $\cos \theta_h^* = \sqrt{1/(1 + \tan^2 \theta_h^*)}$  for  $0 \leq \theta_h^* \leq \pi/2$ .

Note that in the incidence plane (i.e.  $\max(\cos \phi_h^*) = 1$ ), the maximum occurs when  $\theta_h^* = \theta_o^*$ , as expected. However off the incidence plane, we need to explicitly solve for the maximizing angle, because half direction based lobes are not symmetric about the reflection direction. Also note that we require  $\theta_h^*$  be in the range  $0 \leq \theta_h^* \leq \pi/2$ .

Now we select the value from our bounding interval on  $\cos \theta_h^*$  that is closest to the maximizing value given by Equation 31, and plug this along with  $\max(\cos \phi_h^*)$  into Equation 28 to get our desired upper bound on  $(\mathbf{h} \cdot \mathbf{n})$  over the bounding volume  $\mathcal{B}$ .

What we ultimately want is a bound on:

$$f_r^{\text{iso}}(\mathbf{i}, \mathbf{o}) \cos \theta_o = \frac{\rho_s}{4\pi\alpha^2} \sqrt{\frac{\cos \theta_o}{\cos \theta_i}} e^{-\frac{\tan^2 \theta_h}{\alpha^2}} \quad (32)$$

We can put an upper bound on  $\cos \theta_o$  using Equation 27 and we have a upper bound on  $(\mathbf{h} \cdot \mathbf{n})$  which we can convert to a lower bound on  $\tan^2 \theta_h$  using the identity:

$$\tan^2 \theta_h = \frac{1 - (\mathbf{h} \cdot \mathbf{n})^2}{(\mathbf{h} \cdot \mathbf{n})^2} \quad (33)$$

given that  $0 \leq \theta_h \leq \pi/2$ . Putting these together provides the desired bound on the isotropic Ward BRDF.

## 5 Conclusions

In this paper we have discussed the Ward BRDF and several important issues for anyone wanting to use it. We reviewed how to efficiently evaluate and sample the Ward BRDF. We then derived the probability density associated with the Ward sampling scheme

and gave the correct weights to use with the samples. For mathematical correctness, these weights must be used in any Monte Carlo algorithm that uses the Ward sampling.

We also described how to efficiently bound the isotropic Ward BRDF over a set of direction for rendering algorithms that require BRDF bounds.

## References

- ASHIKHMIN, M., AND SHIRLEY, P. S. 2000. An anisotropic phong BRDF model. *Journal of Graphics Tools* 5, 2, 25–32.
- DUER, A. 2005. On the Ward model for global illumination. *not yet published*.
- DUTRE, P., 2001. Global illumination compendium. Web document. <http://www.cs.kuleuven.ac.be/phil/GI/TotalCompendium.pdf>.
- FISHER, F. 1994. R.E versus N.H specular highlights. In *Graphics Gems IV*. 388–400.
- LARSON, G. W., AND SHAKESPEARE, R. 2004. *Rendering with radiance: the art and science of lighting visualization*. Booksurge LLC.
- NGAN, A., DURAND, F., AND MATUSIK, W., 2004. Experimental validation of analytical BRDF models. Technical Sketch, SIGGRAPH 2004. (slides online).
- TORRANCE, K. E., AND SPARROW, E. M. 1967. Theory for offspecular reflection from roughened surfaces. *Journal of the Optical Society of America* 57, 9, 1105–1114.
- WALTER, B., FERNANDEZ, S., ARBREE, A., BALA, K., DONIKIAN, M., AND GREENBERG, D. P. 2005. Lightcuts: A scalable approach to illumination. *ACM Transactions on Graphics* (July). (to appear SIGGRAPH 2005).
- WARD, G. J. 1992. Measuring and modeling anisotropic reflection. In *Computer Graphics (Proceedings of SIGGRAPH 92)*, vol. 26, 265–272.
- WARD, G., 2004. Behavior of materials in radiance. Web document. <http://radsite.lbl.gov/radiance/refer/materials.pdf>.